remote sensing

MDPI

Article

SAR Scatter-Wave Jamming Multiplexing Communication: Based on Small Phase Modulation

Bochang Yu [1], Qidong Zhang [2,*], Guidao Lin [3], Jiaqi Chen [4], Ziyu Huang [4], Gaogao Liu [4], Hongfu Guo [2] and Wen Wu[1]

[1] School of Electro Optics, Nanjing University of Science and Technology, Nanjing 210094, China; 223104131299@njust.edu.cn (B.Y.); wuwen@njust.edu.cn (W.W.)
[2] School of Physics, Xidian University, Xi'an 710071, China; hfguo@xidian.edu.cn
[3] The 723rd Research Institute of China State Shipbuilding Corporation Limited, Yangzhou 225001, China; 25021211567@stu.xidian.edu.cn
[4] School of Electronic Engineering, Xidian University, Xi'an 710071, China; 26021110014@stu.xidian.edu.cn (J.C.); 25021110028@stu.xidian.edu.cn (Z.H.); ggliu@xidian.edu.cn (G.L.)
* Correspondence: 23201110763@stu.xidian.edu.cn

Highlights

What are the main findings?

- This study proposes for the first time a multiplexing communication method for SAR scatter-wave jamming: a method based on slow-time small phase modulation.
- This study demonstrates that the proposed method can achieve reliable information transmission while maintaining effective scatter-wave jamming, with a controllable trade-off between BER performance and azimuth focusing quality.

What are the implications of the main findings?

- SAR scatter-wave jamming signals can be reused as communication carriers, improve spectrum utilization and expand the functionality of SAR electronic countermeasures systems.
- They also provide a theoretical basis for the joint design of jamming performance and embedded communication capabilities in future integrated radar countermeasure systems.

Abstract

This paper proposes a novel jamming multiplexing communication method for synthetic aperture radar (SAR) imaging in scatter-wave jamming (SWJ) scenarios. This method multiplexes communication information by modulating a weak phase in the slow time dimension of the SWJ signal. After receiving the signal, the ground communication station (CS) extracts the information according to the designed algorithm, thus achieving communication transmission. Specifically, a detailed signal model is established to describe the modulation and demodulation mechanism of the communication information. The impact of communication modulation on the SAR image is theoretically analyzed, and the bit error rate (BER) performance of the communication transmission is evaluated. Due to the use of high-gain matched filtering technology in the communication demodulation process, the proposed method achieves better communication BER performance in low signal-to-noise ratio (SNR) environments without significantly reducing jamming performance. Simulation results show that the proposed method achieves reliable information transmission while maintaining effective SWJ capability.

Keywords: synthetic aperture radar; scatter-wave jamming; multiplexed communication; phase modulation; slow time dimension

Check for updates

Academic Editor: Zenghui Zhang

Received: 15 May 2026
Revised: 15 June 2026
Accepted: 24 June 2026
Published: 29 June 2026

Copyright: © 2026 by the authors. Licensee MDPI, Basel, Switzerland. This article is an open access article distributed under the terms and conditions of the Creative Commons Attribution (CC BY) license.

1. Introduction

Synthetic aperture radar (SAR), with its remarkable features of all-weather, all-time and high-resolution imaging, can provide high-resolution ground radar images independent of weather and sunlight, which has led to its widespread application and research in military reconnaissance and civilian detection [1–5]. As the importance of SAR increases, the threat level to important targets is also constantly rising [6]. Therefore, in order to reduce the imaging quality of non-cooperative (NC) SAR and protect the designated area from observation [7], various electronic countermeasure methods (ECMs) against SAR have received widespread attention [8,9].

Depending on whether there is a radiation source inside, the jamming techniques of synthetic aperture radar can be divided into passive and active [10]. Passive jamming generally uses special materials to reflect electromagnetic waves or changes the signal travel conditions to achieve jamming [11]. The most common is the corner reflector, which consists of multiple intersecting metal planes and has a strong rear radar cross-section [12]. However, the electromagnetic scattering characteristics in this type of jamming are fixed, and the ability to modulate the incident wave is very limited [13]. Active jamming is further divided into suppressive and deceptive according to different functions [14–16]. Suppressive jamming involves injects jamming signals into NC radar to drown out the echo signal of the real target. It primarily generates broadband or narrowband active noise signals within the radar's frequency band, radiating them in space to form a suppression jamming environment. By artificially transmitting noise to the radar receiver, it increases the noise level at its input terminal, reduces its signal-to-noise ratio (SNR), and ultimately disrupts the radar's normal operation. This type of jamming can be divided into radio frequency jamming, pulse jamming, amplitude modulation jamming, frequency modulation jamming, and phase modulation jamming, etc. [17]. Although suppression jamming is a common form of SAR jamming, its random noise characteristics result in extremely low correlation with radar echoes. This limits the effectiveness of this type of jamming in the face of modern anti-jamming technology, making it easier to be accurately identified and filtered out [18]. Deceptive jamming, on the other hand, uses jamming pulses to simulate echoes to deceive radar systems, making it impossible for NC radars to correctly distinguish between real and false targets for jamming. This is mainly reflected in the jammer's time delay and phase modulation of the intercepted SAR signal, thereby implanting false scenes or false targets into the real synthetic aperture radar image [19]. Reference [20] proposed a phase error modulation method, which performs two-dimensional precise and controllable intelligent jamming of synthetic aperture radar by setting range and azimuth modulation terms. Reference [21] proposes a method of interrupt sampling repeater jamming to target broadband radar. As a coherent jamming mode, it can generate multiple realistic false targets, but it faces the challenge of not being able to adapt to multiple radar systems with new transmission signals. Similarly, interrupt sampling repeater jamming will generate a main false target that is very similar to the real target, as well as multiple secondary false targets, which have certain regularities and are easy to identify and counter [22,23]. In this regard, reference [24] proposes a method based on sub-Nyquist sampling jamming, which improves the means of template multiplication modulation delay to eliminate or add scatterers on the selected false targets, thereby changing the image shape.

Scatter-wave jamming (SWJ), also known as thermal clutter or terrain scattering jamming, avoids the need for precise modulation of the echo at each point between synthetic aperture pulses. It only requires modulation of the signal at the center of the false scene, which greatly reduces the implementation difficulty [25–27]. Since it simulates the synthetic aperture radar signal to obtain high processing gain, it avoids the large jamming power requirement. At the same time, for bistatic synthetic aperture radar, this method can achieve

better jamming effect [28]. Reference [29] proposes a method for deceiving and jamming the scatter-wave of the antenna process at the displacement phase center to counter the display of ground moving targets by synthetic aperture radar, which reduces the complexity of traditional methods and avoids signal jamming modulation. Reference [30] uses frequency diversity array to realize scatter-wave deceptive jamming, and controls the number of false targets by setting the number of frequency division antennas, but does not analyze the influence of specific frequency offset on the distribution of false targets. Reference [31] proposes a SWJ method based on linear frequency modulated continuous wave integral modulation, claiming that it cannot only jam with traditional SAR, but also with SAR with pulse agility.

However, current work on all jamming techniques focuses primarily on jamming performance, with little research integrating them with other fields. Jamming technology is based on radar development and has many similar configurations to radar, which also makes many radar multiplexing communication technologies applicable to jamming multiplexing communication [32–34]. Therefore, research on jamming and communication multiplexing technologies is not only of great significance in the field of ECM, but can also expand the scope of effective utilization of spectrum resources [35,36]. Regarding SWJ, its scenarios and implementation methods have a natural advantage for jamming multiplexing communication, mainly manifested in that the jamming signal first radiates to the ground scene area, and then reflects to the NC SAR. Therefore, setting the jamming signal radiation area as the communication station (CS) perfectly suits the idea of SWJ-based multiplexing communication. The multiplexed signal is emitted by the jammer, and reaches the ground CS. The information carried by the signal is extracted by the CS to complete the communication task, while the reflected signal completes the jamming task.

2. Contributions of Our Work

In this paper, we focus on the implementation methods of scattering-wave jamming multiplexed communication and its performance trade-off. To the best of the author's knowledge, this is the first study of multiplexing technology that combines SWJ with communication functions. The main contributions of this paper are as follows:

1. For the first time, the application scenario of SWJ is combined with communication requirements, and a method for multiplexing communication based on small phase modulation of SAR scattering-wave jamming is proposed, which provides a new technical approach for jamming systems to realize information transmission while performing jamming tasks.
2. Through rigorous mathematical derivation, the paper presents the difference expressions between the proposed multiplexing method and conventional SWJ in SAR imaging results, theoretically analyzing the mechanism of the jamming effect after multiplexing communication.
3. The paper discusses the limiting factors of the multiplexing method and conducts a trade-off analysis on the overall performance of the proposed method in terms of jamming and communication. It also points out that signal processing methods can greatly improve the SNR performance of communication.
4. Numerical simulations demonstrate the effectiveness and feasibility of the proposed method, verifying that the proposed scatter-wave multiplexing communication method can achieve better bit error rate (BER) performance without significantly reducing jamming performance.

The remainder of this paper is organized as follows: Section 3 introduces the geometric scenario configuration for SWJ multiplexing communication. Section 4 presents the signal model analysis, detailing the design scheme of the jammer's transmitted signal and the

signal processing method at the communication base station receiver. Section 5 compares and analyzes the theoretical differences between this method and conventional SWJ in SAR imaging. Section 6 further discusses the constraints and performance trade-off of the proposed method in terms of jamming and communication. Section 7 demonstrates the performance of the proposed method in terms of SAR imaging jamming effects and communication transmission performance through numerical simulations, thus verifying the feasibility and effectiveness of the method. Finally, Section 8 summarizes the paper.

3. SWJ Multiplexing Communication Geometry Scenario

Figure 1 illustrates the geometry of a jammer simultaneously jamming with the SAR system carried by an Unmanned Aerial Vehicle (UAV) while maintaining communication with a ground target. The UAV carries the SAR platform, employing a forward-looking mode to perform strip imaging of the ground area. The CS is located on the ground to receive information; we use Q to represent its central area. To protect the ground target from UAV detection and promptly transmit information to the CS, the jammer needs the dual capability of jamming with the UAV for protection while simultaneously transmitting information to Q. In this scenario, the UAV platform flies along an ideal straight line at a constant speed v_a, and we set its initial projection onto the ground as the origin O. The direction parallel to the flight path is the X-axis, with the UAV's flight direction being the positive direction. The direction perpendicular to the ground is the Z-axis, with upward being the positive direction. The Y-axis is set according to the right-hand rule.

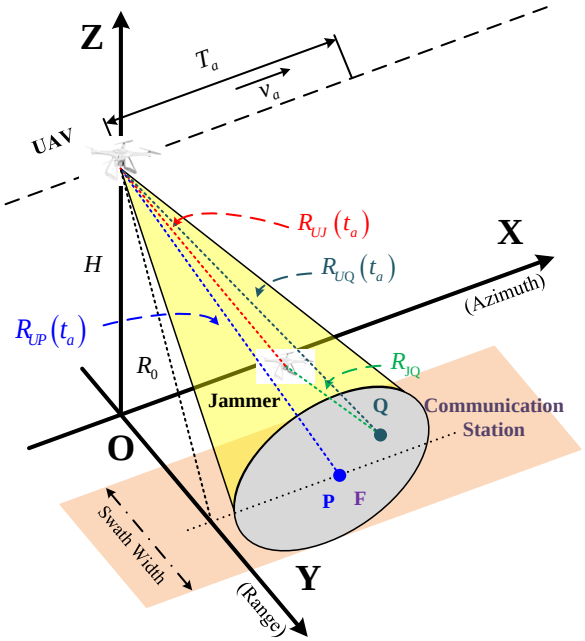


Figure 1. Geometry scene configuration.

The instantaneous position coordinates of the UAV platform are $(v_a t_a, 0, H)$, where t_a is the slow time in the azimuth direction and H is the platform height. P is the point pointed to by the detection beam center at $t_a = 0$, which is also the center of the area to be protected, and its coordinates are $(x_P, y_P, 0)$. Q is within the detection area, and its specific coordinates are $(x_Q, y_Q, 0)$. The jammer is located in the air, with coordinates (x_J, y_J, z_J). It intercepts the SAR signal transmitted by the UAV, modulates and forwards it to the illumination scene centered on Q. The jamming echo scattered by Q appears as a false target F in the SAR image obtained by the UAV. After precise modulation, the false target F can be successfully superimposed on P, thereby completing the protection of P and realizing the jamming

function. At the same time, the signal transmitted by the jammer after modulation also carries communication information. After being received by Q, the signal is demodulated to obtain the corresponding information, thus completing the communication function.

4. Signal Model

4.1. Jammer Transmitted Signal Model

To avoid loss of generality, we assume that the SAR signal transmitted by the UAV is a linear frequency modulated (LFM) signal and its baseband expression can be written as

$$s_U(t_r) = \text{Arect}\left(\frac{t_r}{T_p}\right)\exp\left(j\pi k_r t_r^2 + j\varphi_U\right) \tag{1}$$

where A is the signal amplitude, $rect(\cdot)$ represents the rectangular window function, T_p is the pulse width, and $k_r = B/T_p$ represents the frequency modulation slope, which is determined by the signal bandwidth B and T_p. φ_U is the initial phase of the transmitted signal. Here, we use t_r to represent the fast time concept. After up-conversion, it is transmitted, where the carrier frequency is f_c .

Based on the geometry shown in Figure 1, the vertical slant distance from P to UAV can be obtained as

$$\begin{aligned} R_{UP}(t_a) &= \sqrt{(v_a t_a - x_p)^2 + y_p^2 + H^2} \\ &= \sqrt{R_0^2 + (v_a t_a - x_p)^2} \end{aligned} \tag{2}$$

where R_0 is the initial intercept of the central axis between the UAV and P. The echo from P is obtained by the transmitted signal after a delay of $\frac{2R_{UP}(t_a)}{c}$ and attenuation of α_P, specifically expressed as

$$\begin{aligned} s_P(t_r, t_a) &= \alpha_P(s_U(t_r)\exp(j2\pi f_c t)) \otimes \delta\left(t_r - \frac{2R_{UP}(t_a)}{c}\right) \\ &= A_P \,\text{rect}\left(\frac{t_r - \frac{2R_{UP}(t_a)}{c}}{T_p}\right)\exp\left(j\pi k_r\left(t_r - \frac{2R_{UP}(t_a)}{c}\right)^2 + j\varphi_U\right) \\ &\quad \times \exp\left(j2\pi f_c\left(t_r - \frac{2R_{UP}(t_a)}{c}\right)\right) \end{aligned} \tag{3}$$

Since f_c does not contribute to the imaging processing, the echo is always converted to baseband reception, so Equation (3) becomes

$$\begin{aligned} s_P(t_r, t_a) &= A_P \,\text{rect}\left(\frac{t_r - \frac{2R_{UP}(t_a)}{c}}{T_p}\right)\exp\left(j\pi k_r\left(t_r - \frac{2R_{UP}(t_a)}{c}\right)^2 + j\varphi_U\right) \\ &\quad \times \exp\left(-j2\pi\frac{2R_{UP}(t_a)}{\lambda}\right) \end{aligned} \tag{4}$$

where λ is the wavelength of the SAR signal, and $A_P = \alpha_P A$ is the amplitude of the received signal reflected back. The slant range history corresponding to Q obtained after scattering and retransmission can be expressed as

$$\begin{aligned} R_Q(t_a) &= R_{UJ}(t_a) + R_{JQ} + R_{UQ}(t_a) \\ &= \sqrt{(v_a t_a - x_J)^2 + y_J^2 + (H - z_J)^2} \\ &\quad + \sqrt{(x_J - x_Q)^2 + (y_J - y_Q)^2 + z_J^2} \\ &\quad + \sqrt{(v_a t_a - x_Q)^2 + y_Q^2 + (H - z_Q)^2} \end{aligned} \tag{5}$$

Ignoring the jammer's receive–forward delay, the baseband received echo arriving at the UAV from Q can be expressed by the following:

$$\begin{aligned} s_{\mathrm{Q}}(t_r, t_a) &= \alpha_{\mathrm{Q}}(s_U(t_r)\exp(j2\pi f_c t_r)) \otimes \delta\left(t_r - \frac{R_{\mathrm{Q}}(t_a)}{c}\right) \times \exp(-j2\pi f_c t_r) \\ &= A_{\mathrm{Q}}\,\mathrm{rect}\left(\frac{t_r - \frac{R_{\mathrm{Q}}(t_a)}{c}}{T_p}\right)\exp\left(j\pi k_r\left(t_r - \frac{R_{\mathrm{Q}}(t_a)}{c}\right)^2 + j\varphi_U\right) \\ &\quad \times \exp\left(-j2\pi\frac{R_{\mathrm{Q}}(t_a)}{\lambda}\right) \end{aligned} \tag{6}$$

where α_{Q} is the attenuation factor corresponding to Q, and $A_{\mathrm{Q}} = \alpha_{\mathrm{Q}}A$ is the amplitude of the received signal reflected at Q. To generate the corresponding false target F at P, modulation can be performed based on the phase difference generated by the distance:

$$\begin{aligned} s_F(t_r, t_a) &= G_J s_{\mathrm{Q}}(t_r, t_a) \otimes \delta\left(t_r - \frac{2R_{UP}(t_a) - R_{\mathrm{Q}}(t_a)}{c}\right) \\ &\quad \times \exp\left(-j2\pi\frac{2R_{UP}(t_a) - R_{\mathrm{Q}}(t_a)}{\lambda}\right) \\ &= G_J s_{\mathrm{Q}}(t_r, t_a) \otimes \delta\left(t_r - \frac{\Delta R_{\mathrm{Q}P}(t_a)}{c}\right) \times \exp\left(-j2\pi\frac{\Delta R_{\mathrm{Q}P}(t_a)}{\lambda}\right) \end{aligned} \tag{7}$$

where $\otimes$ represents the convolution operation, G_J is the jamming gain factor of the corresponding signal from the jammer, and $\Delta R_{\mathrm{Q}P}(t_a) = 2R_{UP}(t_a) - R_{\mathrm{Q}}(t_a)$ is the distance difference between the echoes from the two positions, which is also the jamming parameter value that the jammer needs to modulate. We only need to carefully adjust G_J and $\Delta R_{\mathrm{Q}P}(t_a)$ to make the generated target at F cover the real target at P, thus completing the jamming echo of the scatter-wave.

Based on the echo signal required for jamming, we can obtain the expression for the baseband signal transmitted by the jammer that does not carry communication information as follows:

$$\begin{aligned} s_J(t_r, t_a) = &\left(\begin{array}{l} G_J\,\mathrm{rect}\left(\dfrac{t_r - \dfrac{R_{UJ}(t_a)}{c}}{T_p}\right) \\ \quad \times \exp\left(j\pi k_r\left(t_r - \dfrac{R_{UJ}(t_a)}{c}\right)^2 + j\varphi_U\right) \\ \quad \times \exp\left(-j2\pi\dfrac{R_{UJ}(t_a)}{\lambda}\right) \end{array}\right) \\ &\otimes \delta\left(t_r - \frac{\Delta R_{\mathrm{Q}P}(t_a)}{c}\right) \times \exp\left(-j2\pi\frac{\Delta R_{\mathrm{Q}P}(t_a)}{\lambda}\right) \end{aligned} \tag{8}$$

For the jammer, its transmitted signal beam is directed at Q. It can send composite signals carrying communication information to perform jamming while simultaneously completing its communication task. With the continuous improvement of DRFM, the SWJ can be modulated to carry communication information so that the form of the signal transmitted to Q can be artificially controlled. We can embed the communication information in the slow time dimension, where the information bits use an NRZ sequence and small phase keying is used for phase generation:

$$\phi_{t_a} = \varepsilon b_{t_a}, \qquad 0 < \varepsilon \ll 1 \tag{9}$$

where $b_{t_a} \in \{+1, -1\}$. Therefore, the model of the forwarded *kth* jamming pulse signal can be expressed as

$$s_{JC}(t_r, t_a) = s_J(t_r, t_a) \exp(j\phi_{t_a}) \exp(j2\pi f_c t_r) \tag{10}$$

4.2. Signal Receiving and Processing Model for Q

For Q, the received signal consists of two parts: the SAR signal transmitted by the UAV and the composite signal carrying communication information relayed by the jammer. Since both the UAV and the jammer are in the air and Q is on the ground, its line-of-sight (LOS) path constitutes the majority of the signal. Therefore, we can reasonably assume that the receiving channel is single path. Thus, the overall received signal model for Q is

$$\begin{aligned} r_{\mathrm{Q}}(t_r, t_a) = {} & \alpha_{UQ}(s_U(t_r) \exp(j2\pi f_c t)) \otimes \delta\left(t_r - \frac{R_{UQ}(t_a)}{c}\right) \\ & + \alpha_{JQ} s_{JC}(t_r, t_a) \otimes \delta\left(t_r - \frac{R_{JQ}}{c}\right) + n(t_r, t_a) \end{aligned} \tag{11}$$

where α_{UQ} is the attenuation factor from the UAV to Q, α_{JQ} is the attenuation factor from the jammer to Q, and $n(t_r, t_a)$ is complex Additive White Gaussian Noise (AWGN) following a $N(0, \sigma^2)$ distribution. To extract the corresponding communication information, we first need to perform down-conversion and matched filtering on $r_{\mathrm{Q}}(t_r, t_a)$. The matched filter used here is $h(t_r) = {s_U}^*(-t_r)$, where $*$ is the conjugate filter. The resulting processed output is

$$\begin{aligned} c_{\mathrm{Q}}(t_r, t_a) = {} & (r_{\mathrm{Q}}(t_r, t_a) \times \exp(-j2\pi f_c t_r)) \otimes h(t_r) \\ = {} & \left(\begin{array}{l} \alpha_{UQ} A \,\mathrm{rect}\left(\dfrac{t_r - \dfrac{R_{UQ}(t_a)}{c}}{T_p} \right) \\ \quad \times \exp\left(j\pi k_r \left(t_r - \dfrac{R_{UQ}(t_a)}{c} \right)^2 + j\varphi_U \right) \\ \quad \times \exp\left(-j2\pi f_c \dfrac{R_{UQ}(t_a)}{c} \right) \end{array} \right) \otimes h(t_r) \\ & + \left(\begin{array}{l} \alpha_{JQ} G_J \left(\alpha_{UJ} A \,\mathrm{rect}\left(\dfrac{t_r - \dfrac{\Delta R_{QP}(t_a)}{c} - \dfrac{R_{UJ}(t_a)}{c}}{T_p} \right) \right) \\ \quad \times \exp\left(j\pi k_r \left(t_r - \dfrac{\Delta R_{QP}(t_a)}{c} - \dfrac{R_{UJ}(t_a)}{c} \right)^2 + j\varphi_U \right) \\ \quad \times \exp\left(-j2\pi f_c \left(\dfrac{\Delta R_{QP}(t_a)}{c} + \dfrac{R_{UJ}(t_a)}{c} \right) \right) \\ \quad \times \exp(j\phi_{t_a}) \end{array} \right) \otimes h(t_r) \\ & + n(t_r, t_a) \otimes h(t_r) \end{aligned} \tag{12}$$

The second term in Equation (12) represents the content that ground CS need to focus on. Expanding it, we can obtain

$$\begin{aligned} c_{\mathrm{Q}}(t_r, t_a) \approx {} & \alpha_{JQ} G_J \alpha_{UJ} \exp(j\varphi_U) \\ & \times \exp\left(-j2\pi f_c \left(\frac{\Delta R_{QP}(t_a) + R_{UJ}(t_a)}{c} \right) \right) \exp(j\phi_a) \\ & \times A^2 \,\mathrm{sinc}\left(B \left(t_r - \frac{\Delta R_{QP}(t_a) + R_{UJ}(t_a)}{c} \right) \right) \\ = {} & C_J(t_a) \exp(j\phi_{t_a}) \chi(t_r, t_a) \end{aligned} \tag{13}$$

where $\mathrm{C}_J(t_a) = \alpha_{JQ} G_J \alpha_{UJ} A^2 \exp(j\varphi_U) \exp\left(-j2\pi f_c \left(\frac{\Delta R_{QP}(t_a) + R_{UJ}(t_a)}{c} \right) \right)$ can be viewed as a function of attenuation factor, jammer gain, initial phase of transmitted signal and

coefficients related to slow time. $\chi(t_r, t_a)$ is the product of the $\sin c(\cdot)$ function obtained after matched filtering and the residual phase. Therefore, for the communication information, it can be rewritten as an estimable model:

$$\widetilde{c}_{\mathrm{Q}}(t_r, t_a) = C_J(t_a)\exp(j\phi_{t_a})\chi(t_r, t_a) + \widetilde{n}(t_r, t_a) \tag{14}$$

For Equation (14), in order to estimate the value of $\exp(j\phi_{t_a})$, we first need to extract peak point information in each slow time dimension. Let $t_r = \frac{\Delta R_{QP}(t_a)+R_{UJ}(t_a)}{c}$. The equivalent observation model can be obtained:

$$\widetilde{c}_{\mathrm{Q}}(t_a) = C_J(t_a)\exp(j\phi_{t_a}) + \widetilde{n}(t_a) \tag{15}$$

Now, the problem of extracting communication information $\widetilde{c}_{\mathrm{Q}}(t_a)$ transforms into estimating the phase symbol $\exp(j\phi_{t_a})$ from under the condition of amplitude $C_J(t_a)$. It should be noted that the added communication information has the constraint condition of Equation (9), so for Equation (15), a binary decision can be performed to obtain the corresponding communication information data. $C_J(t_a)$ includes the amplitude of the signal, the delay phase caused by distance and the additional phase caused by matched filtering. The part that has the main influence on the decision is the phase effect, so we need to estimate and compensate for this part. Let its expression be

$$\exp\left(j\theta(t_a)\right) = \exp(j\varphi_U)\exp\left(-j2\pi f_c\left(\frac{\Delta R_{QP}(t_a) + R_{UJ}(t_a)}{c}\right)\right) \tag{16}$$

This phase change is mainly caused by the motion of the UAV, and the specific position of the drone can be obtained through methods such as positioning and fitting. However, the geometric compensation used for positioning and fitting can cause significant phase estimation errors and the accuracy of phase compensation directly affects the performance of demodulation. We assume that the equivalent path error after geometric compensation is R_{eq}; the magnitude of the phase error caused by this term is

$$\Delta\varphi = \frac{2\pi}{\lambda}R_{eq} \tag{17}$$

For BPSK hard decision, the residual phase error is usually required to be smaller than $\frac{\pi}{4}$. Therefore, the following constraints can be obtained:

$$\Delta\varphi < \frac{\pi}{4} \tag{18}$$

Thus, the minimum positioning error range can be obtained:

$$R_{eq} < \frac{\lambda}{8} \tag{19}$$

For high-frequency signals, this value is on the order of centimeters. This result indicates that if only geometric positioning is used for phase compensation, centimeter-level equivalent path accuracy is required. Therefore, the UAV positioning information is mainly used to provide a coarse phase model, while the residual phase error should be further estimated and compensated by pilot assisted phase tracking. Therefore, the overall estimation of $\exp(j\theta(t_a))$ is achieved using pilot signals. For a known segment $\exp(j\phi_{t_a})$, the least squares estimation of the influencing phase can be obtained as follows:

$$\widehat{\theta}(t_a) = \arg\left(\sum_{t_a} \widetilde{c}_{\mathrm{Q}}(t_a)\exp(-j\phi_{t_a})\right) \tag{20}$$

After phase compensation, we can obtain

$$\widehat{c}_{\mathrm{Q}}(t_a) = \widetilde{c}_{\mathrm{Q}}(t_a)\exp\left(-j\widehat{\theta}(t_a)\right) = \widehat{A}\exp(j\phi_{t_a}) + \widehat{n}(t_a) \tag{21}$$

where $\widehat{A} = \alpha_{JQ}G_J\alpha_{UJ}A^2$ is the equivalent amplitude. Then, performing an Euler transform on $\exp(j\phi_a)$ yields

$$\exp(j\phi_{t_a}) = \cos(b_{t_a}\varepsilon) + j\sin(b_{t_a}\varepsilon) \tag{22}$$

Since b_{t_a} is an NRZ sequence, Equation (22) can be transformed into

$$\exp(j\phi_{t_a}) = \cos\varepsilon + jb_{t_a}\sin\varepsilon \tag{23}$$

Substituting Equation (23) into Equation (21) yields

$$\begin{aligned}\widehat{c}_{\mathrm{Q}}(t_a) &= \widehat{A}(\cos\varepsilon + jb_{t_a}\sin\varepsilon) + \widehat{n}(t_a)\\ &= \widehat{A}\cos\varepsilon + j\widehat{A}b_{t_a}\sin\varepsilon + \widehat{n}(t_a)\end{aligned} \tag{24}$$

For Equation (24), the real part does not contain anything related to communication information, so we take its imaginary part:

$$\mathrm{Im}\left(\hat{c}_{\mathrm{Q}}(t_a)\right) = \hat{A}b_{t_a}\sin\varepsilon + \mathrm{Im}(\hat{n}(t_a)) \tag{25}$$

The transmitted communication bits can be estimated using hard decision estimation as follows:

$$\hat{b}_{t_a} = sign\left(\mathrm{Im}\left(\hat{c}_{\mathrm{Q}}(t_a)\right)\right) \tag{26}$$

where $sign(\cdot)$ represents the sign function, used to determine the sign of the corresponding function variable. Its specific expression is

$$\mathrm{sign}(x) = \begin{cases} +1, & x > 0 \\ 0, & x = 0 \\ -1, & x < 0 \end{cases} \tag{27}$$

After overall reception processing, the final communication information transmission is completed. It should be noted that Equation (25) directly corresponds to the value of the modulation bit. The result obtained by hard decision is equivalent to the maximum likelihood decision.

5. Imaging Reception and Processing

5.1. Imaging Processing Without Communication Information

To analyze the imaging jamming results of the UAV before and after adding communication information, we first derive the traditional SWJ imaging processing results. In this case, the overall baseband echo obtained by the UAV consists of two parts: the echo of the real target P and the echo of the false target F. The specific expression is as follows:

$$\begin{aligned} s(t_r,t_a) &= s_P(t_r,t_a) + s_F(t_r,t_a) \\ &= A_P \,\mathrm{rect}\left(\frac{t_r - \frac{2R_{UP}(t_a)}{c}}{T_p}\right) \\ &\quad \times \exp\left(j\pi k_r \left(t_r - \frac{2R_{UP}(t_a)}{c}\right)^2 + j\varphi_U\right) \\ &\quad \times \exp\left(-j2\pi \frac{2R_{UP}(t_a)}{\lambda}\right) \\ &\quad + G_J s_Q(t_r,t_a) \otimes \delta\left(t_r - \frac{\Delta R_{QP}(t_a)}{c}\right) \\ &\quad \times \exp\left(-j2\pi \frac{\Delta R_{QP}(t_a)}{\lambda}\right) \end{aligned} \tag{28}$$

For UAV imaging processing, the first term of Equation (28) is not included in the scope of this paper because it is the echo signal of a point target without jamming, and the corresponding result can be obtained according to the reasonable processing procedure of SAR. The second term is the SWJ signal, which is the focus of this paper.

The RD algorithm usually converts the echo jamming signal into a SAR jamming imaging through two steps: range and azimuth compression. First, range matched filtering is performed; the corresponding filter is

$$h_r(t_r) = A_{\mathrm{ref}} \,\mathrm{rect}\left(\frac{t_r}{T_p}\right) \exp\left(-j\pi k_r t_r^2\right) \tag{29}$$

where A_{ref} is the reference amplitude. The result of the jamming term after range matched filtering is expressed as

$$\begin{aligned} s_{Fr}(t_r,t_a) &= s_F(t_r,t_a) \otimes h_r(t_r) \\ &= G_J A_Q A_{\mathrm{ref}} \exp\left(-j\frac{2\pi}{\lambda}\left(\Delta R_{QP}(t_a) + R_Q(t_a)\right)\right) \exp(j\varphi_U) \\ &\quad \times \mathrm{sinc}\left(B\left(t_r - \frac{R_Q(t_a)}{c} - \frac{\Delta R_{QP}(t_a)}{c}\right)\right) \end{aligned} \tag{30}$$

From Equation (30), it can be seen that when the modulation is precise, the corresponding F range compression position is at P. To obtain the azimuth result, we perform the Fast Fourier Transform (FFT) on the azimuth time of the range compressed signal and can obtain

$$S_{Fr}(t_r,f_a) = \int s_{Fr}(t_r,t_a) \exp(-j2\pi f_a t_a)\, dt_a \tag{31}$$

Therefore, the azimuth matched filter can be written as

$$H_a(f_a;R_0) = \exp\left(j\pi \frac{f_a^2}{k_a(R_0)}\right) \tag{32}$$

where $k_a(R_0) = \frac{2v_a^2}{\lambda R_0}$ is the azimuth frequency modulation slope, which is determined by the UAV's flight speed v_a and slant range R_0 . After range migration correction and azimuth compression, the final imaging expression is

$$S_F(t_r,t_a) = \mathrm{IFFT}\left(S_{Fr}(t_r,f_a)\, H_{RCMC}(f_a)\, H_a(f_a;R_0)\right) \tag{33}$$

where $H_{RCMC}(f_a)$ is the range migration correction model and IFFT$(\cdot)$ is the inverse FFT. As described earlier, the key modulation parameters for jamming are G_J and $\Delta R_{QP}(t_a)$. And proper settings can generate a jamming image covering the real target point P.

5.2. Imaging Containing Communication Information

Equation (33) gives the conventional jamming imaging results without added communication information. As can be seen from Equation (10), the added communication information exists in the slow time dimension, not the fast time dimension. Therefore, it does not affect the range imaging process, and the main impact is on the azimuth direction. The expression after range compression is transformed from Equation (30) into

$$s_{Fcr}(t_r, t_a) = s_{Fr}(t_r, t_a) \exp\left(j\phi_{t_a}\right) \tag{34}$$

Using the definition of Equation (23), Equation (34) can be approximated as

$$s_{Fcr}(t_r, t_a) = s_{Fr}(t_r, t_a) \cos\varepsilon + s_{Fr}(t_r, t_a) j b_{t_a} \sin\varepsilon \tag{35}$$

Similarly, applying azimuth compression to Equation (35) and using the same filter as Equation (32), the final imaging result containing communication information can be obtained as follows:

$$S_{Fc}(t_r, t_a) = S_F(t_r, t_a) \cos\varepsilon + \text{IFFT}(\text{FFT}(s_{Fr}(t_r, t_a) j b_{t_a} \sin\varepsilon) H_{RCMC}(f_a) H_a(f_a; R_0)) \tag{36}$$

where FFT$(\cdot)$ is the Fast Fourier Transform. The first term in Equation (36) represents the traditional SWJ imaging component scaled by $\cos(\varepsilon)$, which preserves the coherent accumulation characteristics of the original azimuth. The second term represents the imaging component caused by communication information due to changes along the slow time dimension, destroys some azimuthal coherence, and is mapped to defocused energy or sidelobe components after azimuthal matching filtering.

6. Performance Analysis

6.1. Changes in Jamming Performance

According to Equation (36), the impact of ε on jamming images can be analyzed from two aspects: firstly, the peak energy loss of coherent accumulation term, and secondly, the sidelobe spurious amount of incoherent accumulation.

We can abstract the coherent accumulation of conventional SAR as

$$I_F(t_r, t_a) \propto \sum_{n=0}^{N-1} w_n \tag{37}$$

where $n = 0, 1, \cdots, N-1$ represents discrete points of slow time length T_a; its size is the same as the number of pulse repetitions. w_n can be understood as the actual weight value formed by the transmitted signal window function, antenna pattern and range attenuation. In general, $w_n = 1$. Therefore, the result without communication information can be equivalent to

$$I_F(t_r, t_a) \propto N \tag{38}$$

So the scaled coherent focusing component is

$$I_{Fc}(t_r, t_a) \propto N \cos\varepsilon \tag{39}$$

Therefore, the amplitude loss of the main peak coherent component is

$$\Delta_m = 20\log_{10}\left(\frac{I_{Fc}(t_r,t_a)}{I_F(t_r,t_a)}\right) = 20\log_{10}(\cos\varepsilon) \tag{40}$$

As can be seen from Equation (40), the main peak attenuation is related to the ε value of the added communication information phase. For the uncorrelated accumulation of sidelobe noise caused by communication information in imaging results, we can expand it as follows:

$$\mathrm{IFFT}(\mathrm{FFT}(s_{Fr}(t_r,t_a)jb_{t_a}\sin\varepsilon)H_{RCMC}(f_a)H_a(f_a;R_0)) = j\sin\varepsilon\int s_{Fr}(t_r,\xi)b_\xi h(t_a-\xi)d\xi \tag{41}$$

where $h(t_a)$ is the overall time domain filter expression corresponding to the combination of range migration and azimuth filter. Since b_{t_a} is an NRZ sequence, the result of Equation (41) can be understood as mapping b_{t_a} to the defocused structure of the imaging result through the filter $h(t_a)$, which leads to the lifting of the azimuth sidelobe and the diffusion of phase noise. And the magnitude of the sidelobe lift caused by this can also be abstracted as

$$\Delta_s = 20\log_{10}(\sin\varepsilon) \tag{42}$$

6.2. Communication Performance

For communication, the decision is determined by Equation (26), which can be equivalent to a one-dimensional BPSK decision. The corresponding theoretical BER is

$$\mathrm{BER} = Q\left(\frac{\widehat{A}\sin\varepsilon}{\sqrt{\sigma^2/2}}\right) = Q\left(\sqrt{\frac{2\widehat{A}^2}{\sigma^2}}\sin\varepsilon\right) \tag{43}$$

It's important to note that $\widehat{A}$ here refers to the equivalent amplitude, not the received signal amplitude. The main difference lies in the signal processing gain of Q after matched filtering. Based on this, the received signal SNR can be defined as

$$\frac{\widehat{A}^2}{\sigma^2} = (B\cdot T)^2\,\mathrm{SNR} \tag{44}$$

where $B\cdot T$ is the time–bandwidth product, which is the pulse compression gain. Then, we can obtain the relationship between BER and SNR from $\varepsilon \ll 1$ as follows:

$$\mathrm{BER} \approx Q\left(\varepsilon\sqrt{2(B\cdot T)^2\,\mathrm{SNR}}\right) \tag{45}$$

7. Simulation Results

7.1. Simulation Parameter Settings

To demonstrate the feasibility of the method proposed in this paper, simulation experiments are conducted for the application scenario shown in Figure 1 in this section. The specific parameter settings are given in Table 1.

The method proposed in this paper utilizes signals that possess both jamming and communication capabilities. Therefore, we conducted simulation experiments separately for these two functions. Firstly, we simulated UAV imaging to explore the jamming results of the signals. Subsequently, we simulated the ground communication base stations to verify the communication capabilities.

Table 1. Simulation Parameter Settings.

Parameters	Values
Carrier Frequency	3 GHz
Bandwidth	100 MHz
Pulse Width	1.5 us
UAV Speed	100 m/s
UAV Altitude	200 m
Centre Distance	10 km
Length of Synthetic Aperture	400 m
Pulse Repetition Frequency	400 Hz
Jammer Height	50 m
ε Value	0.1, 0.5, 0.8
Data Bits	1536
Pilot Bits	64
Monte Carlo	500

7.2. Jamming Performance Simulation

We conducted imaging experiments on the UAV under three conditions to explore the jamming performance of the method proposed in this paper: without jamming, conventional SWJ, and SWJ with added communication information. Based on the data provided in Table 1, the UAV imaging result in the absence of jamming is shown in Figure 2. The protected area P, the jammer and the communication base station Q (with the yellow rectangular box indicating the communication base station area and the center of the box representing the base station itself) are clearly visible. Subsequently, simulation experiments were conducted using traditional SWJ under the same parameters. We define the Jamming Signal Ratio (JSR) as the power ratio of the jamming signal echo at the SAR receiver to the true radar signal echo, and set it to 10 dB. The resulting UAV imaging is shown in Figure 3. In this figure, the yellow rectangular box still represents the communication base station Q area, while the white rectangular box indicates the false target imaging results in the jammed area. As the signal forwarded by the jammer is modulated based on the communication base station Q, the imaging results of the surrounding scattering points are no longer standard translations but are shifted according to different distances, as specifically shown within the white rectangular box in Figure 3. Now, the protected target P is successfully covered by the false target, achieving the desired jamming effect.

We conducted simulation experiments with communication addition by setting the parameter ε to 0.1 under the same parameter configuration to demonstrate the feasibility and effectiveness of the proposed method. The resulting UAV imaging is shown in Figure 4, where the content within the rectangular box remains consistent with that in Figure 3. Compared with Figure 3, it can be observed that the proposed method still achieves satisfactory jamming performance. According to the analysis of Equations (36) and (41), when ε becomes larger, the sidelobes in the azimuth direction of SAR imaging are uplifted and the peak of the main lobe is reduced, which is primarily reflected in the variation of the peak sidelobe level. To validate this result, we increased ε and conducted the same experiment, obtaining the results shown in Figure 5. Figures 5a and 5b present the imaging results for $\varepsilon = 0.5$ and $\varepsilon = 0.8$, respectively. A comparison of the two subfigures reveals that as ε increases, the azimuth direction of the false target broadens, covering the entire azimuth direction, while no significant change is observed in the range direction. This is

specifically attributed to the failure of coherent accumulation of the signal, leading to a mismatch in azimuth matched filtering, which is consistent with the previous analysis.

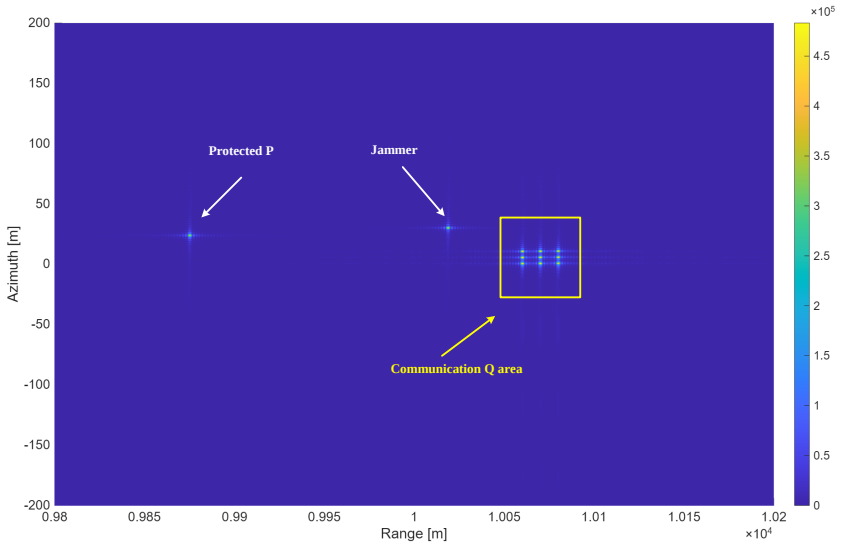


Figure 2. Imaging result without jamming.

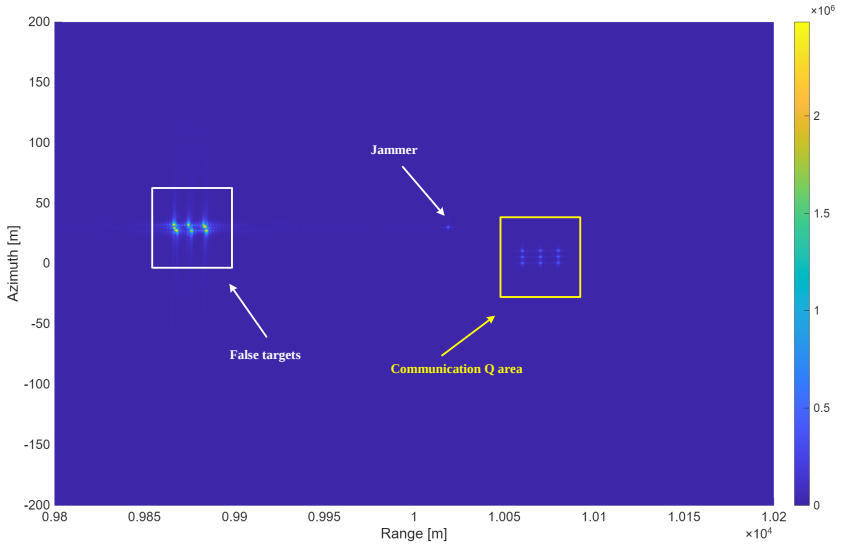


Figure 3. Imaging result of conventional SWJ.

To obtain a more detailed comparison of the results, we present the range and azimuth profiles of the protected P in the aforementioned imaging results. First, the range profiles are shown in Figure 6. Specifically, Figure 6a displays the range profile of P in the absence of jamming. Figure 6b shows the result under conventional SWJ. And Figures 6c, 6d and 6e present the results under SWJ with multiplexing communication information for $\varepsilon = 0.1$, $\varepsilon = 0.5$ and $\varepsilon = 0.8$, respectively. Comparing Figures 6a and 6b, it can be seen that multiple false targets appear around P under conventional SWJ, indicating the successful achievement of deceptive jamming. According to the analysis of Equation (34), the inclusion of communication information has almost no impact on range jamming. A comparison of Figures 6b, 6c, 6d and 6e reveals that the false targets in the range dimension persist and the ratio between the main lobe and its surrounding sidelobes remains constant, which aligns with the theoretical analysis.

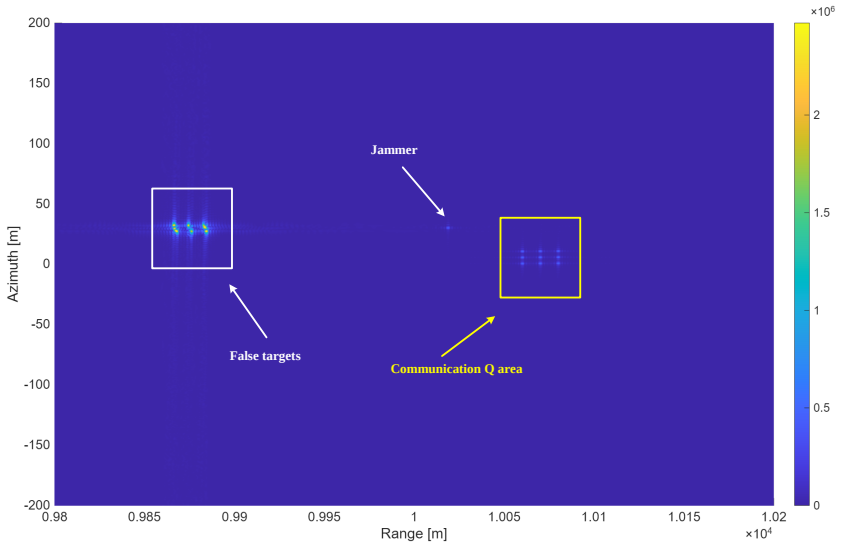
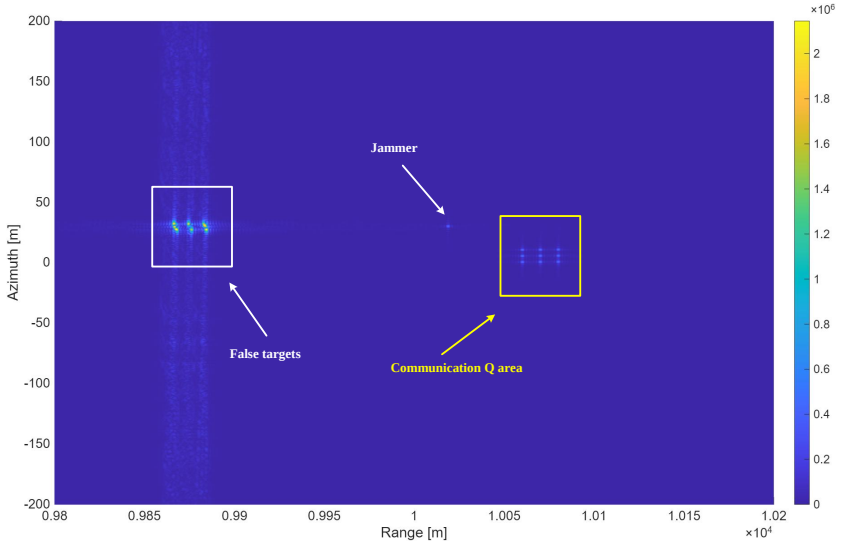
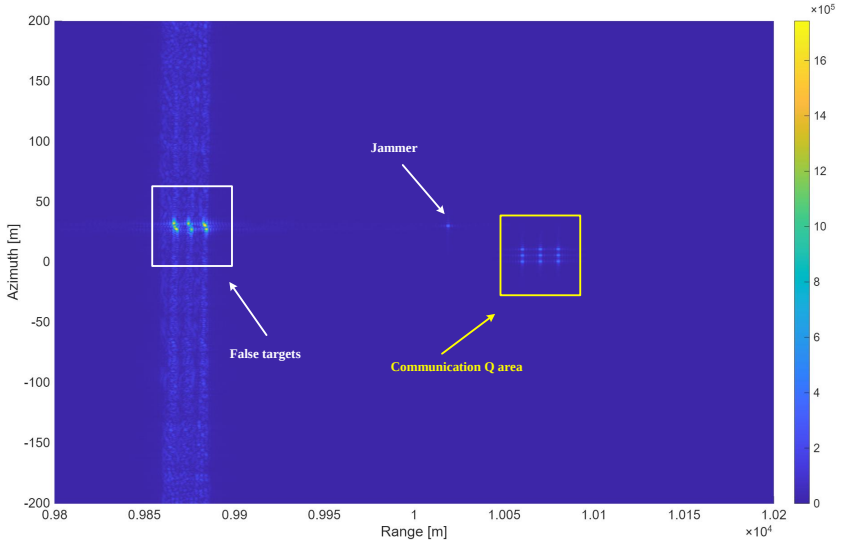


Figure 4. Imaging result of SWJ modulated with communication information.



(**a**)



(**b**)

Figure 5. Imaging result under the higher ε: (**a**) Result with $\varepsilon = 0.5$; (**b**) result with $\varepsilon = 0.8$.

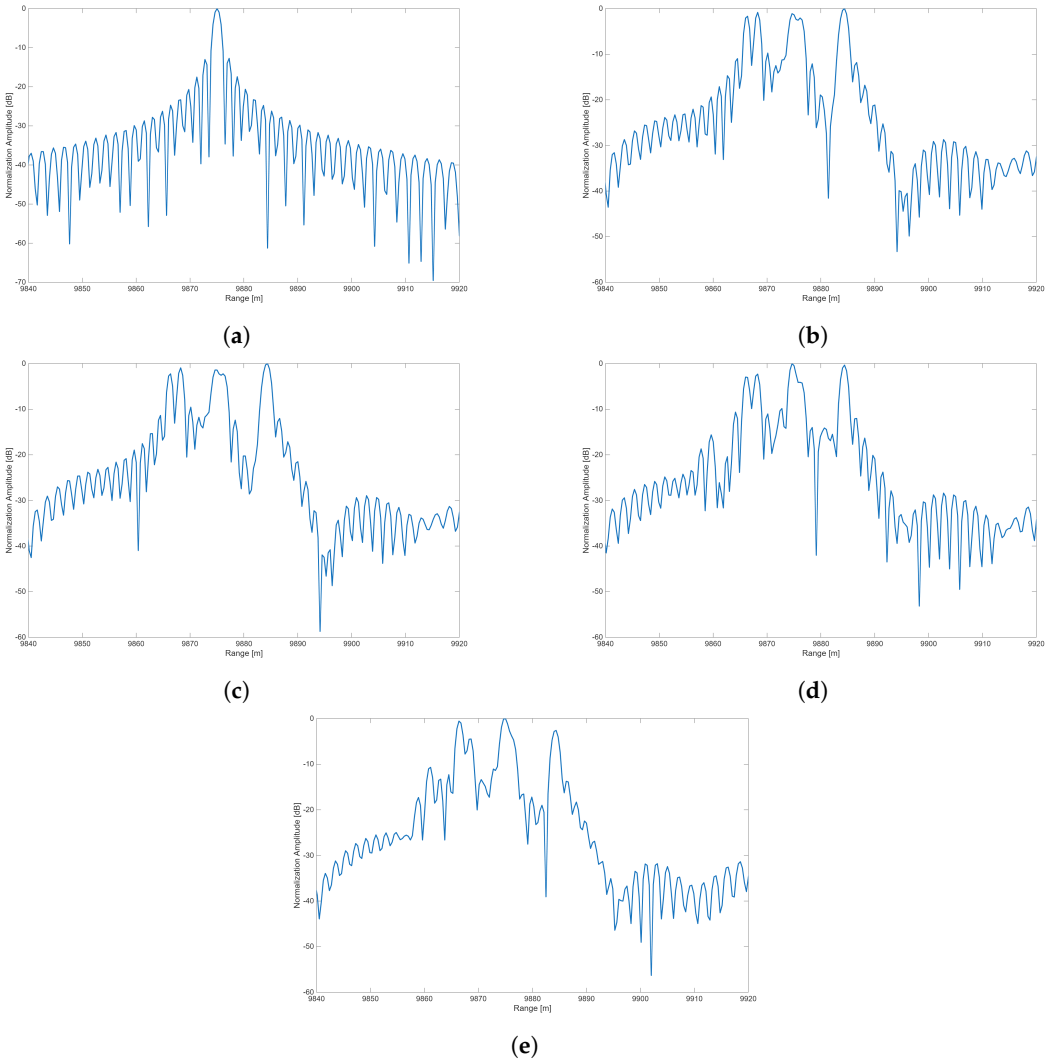


Figure 6. Range profiles of the protected area: (**a**) Without jamming; (**b**) conventional SWJ; (**c**) SWJ with $\varepsilon = 0.1$; (**d**) SWJ with $\varepsilon = 0.5$; (**e**) SWJ with $\varepsilon = 0.8$.

The azimuth profiles are shown in Figure 7. Specifically, Figure 7a displays the azimuth profile of P in the absence of jamming, Figure 7b shows the result under conventional SWJ. Figures 7c, 7d and 7e present the jamming results with multiplexing communication information for $\varepsilon = 0.1$, $\varepsilon = 0.5$ and $\varepsilon = 0.8$, respectively. From Figure 7a,b, it can be seen that multiple false targets also appear in the azimuth direction when SWJ is present. When communication information is multiplexed, multiple false targets similarly appear, also achieving the deceptive jamming function. However, as ε increases, the ratio between the main lobe and the surrounding sidelobes in the false target coverage area changes significantly. When ε increases from 0.1 to 0.8, this ratio decreases from 30 dB to 15 dB, which aligns with the analysis in Section 6, that is, as the communication capability increases, the jamming effect significantly degrades.

The simulation results demonstrate the inherent trade-off between jamming performance and communication performance in the proposed SWJ multiplexing communication method. The modulation parameter ε determines the phase separation between two signals. A larger ε increases the useful decision component of the received communication signal, which is beneficial for improving BER performance. However, from the perspective of SAR imaging, larger ε can also introduce stronger slow-time phase perturbations in SWJ signals. Therefore, the coherent accumulation in the azimuth direction is weakened, resulting in azimuth defocusing, sidelobe elevation and a decrease in the pea- to-sidelobe ratio of

the jamming image. Therefore, ε should not increase indefinitely. On the contrary, the choice should be made based on the required trade-off between communication reliability and jamming image focusing quality. In the considered simulation, $\varepsilon = 0.1$ can provide acceptable communication performance while maintaining good azimuth focusing quality, while $\varepsilon = 0.5$ and $\varepsilon = 0.8$ are mainly used to illustrate the degradation trend under stronger communication modulation.

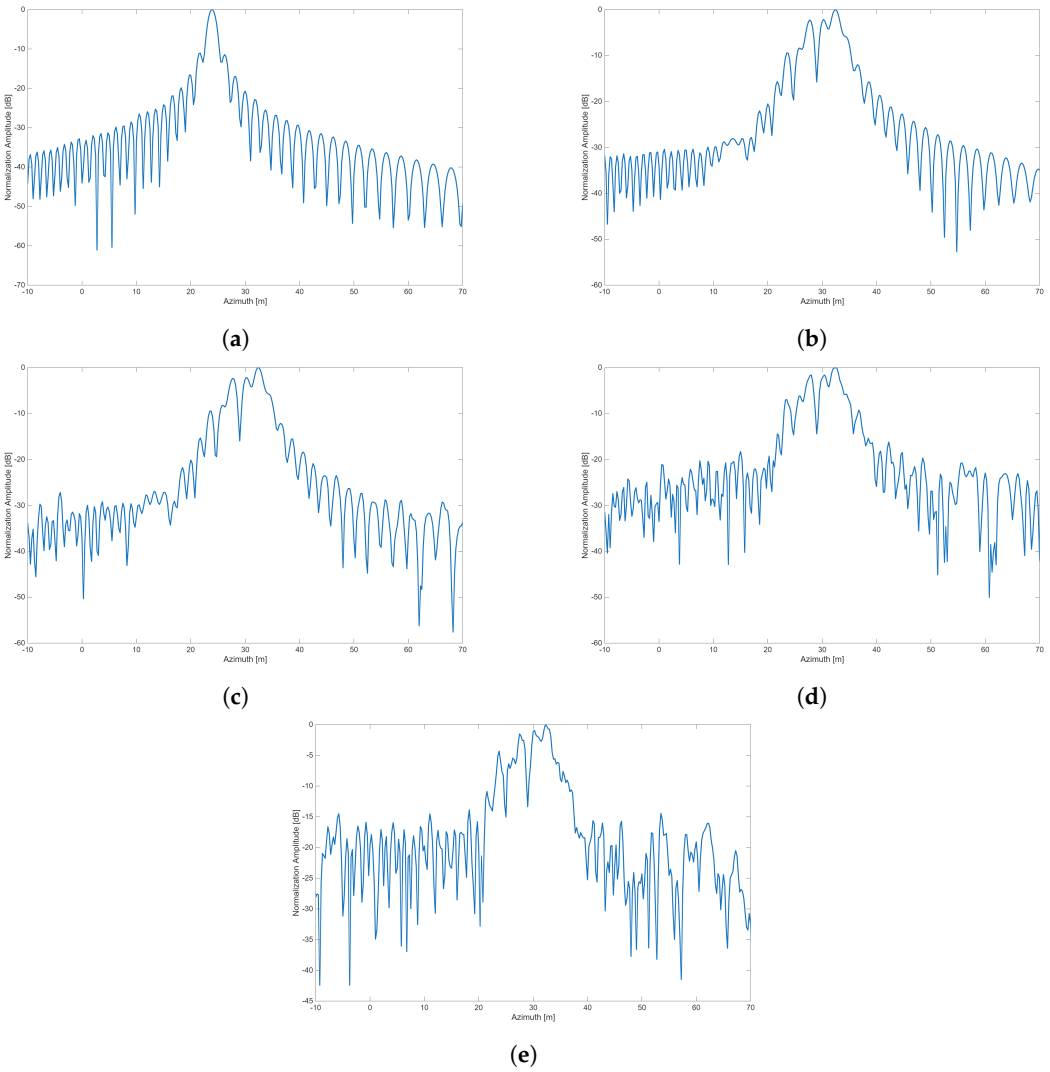


Figure 7. Azimuth profiles of the protected area: (**a**) Without jamming; (**b**) conventional SWJ; (**c**) SWJ with $\varepsilon = 0.1$; (**d**) SWJ with $\varepsilon = 0.5$; (**e**) SWJ with $\varepsilon = 0.8$.

7.3. Communication Performance Simulation

Theoretical analysis of jamming performance and simulation experimental results indicate that the value of ε affects the jamming effectiveness. To verify the communication performance results under realistic conditions suitable for practical applications, simulation experiments were first conducted with $\varepsilon = 0.1$. Based on the parameters given in Table 1, the total transmitted data volume in this scenario is calculated to be 1600 bits. To compensate for communication information, 64 pilot symbols are uniformly inserted over the 1600 slow-time samples. On this basis, 500 Monte Carlo experiments were performed to obtain the BER results of the proposed method, which were then compared with the theoretical BER results from Equation (45), yielding the results shown in Figure 8. In the figure, the blue circular line represents the theoretical BER results calculated by Equation (45), while the red cross line represents the BER results obtained from Monte Carlo experiments. A comparison

of the two curves shows that the experimental results closely match the theoretical results. When the SNR at the communication receiving base station is -5 dB, the BER is below 10^{-3}.

To verify the influence of ε on the BER performance, we concurrently set up cases with $\varepsilon = 0.5$ and $\varepsilon = 0.8$, and conducted the same Monte Carlo experiments, with the results shown in Figure 9. In the figure, the blue diamond line represents the result for 0.1, the red triangle dashed line represents the result for 0.5 and the yellow pentagram dotted line represents the result for 0.8. It can be observed that as ε increases, the communication BER performance also improves. When ε is greater than 0.5, the BER can fall below 10^{-3} at an SNR of -15 dB. Additionally, the following conclusion can be drawn from the figure: for large value ε, even if it is increased, the BER performance will not be significantly improved. Meanwhile, the BER performance for $\varepsilon = 0.1$ is sufficient to adapt to most environments.

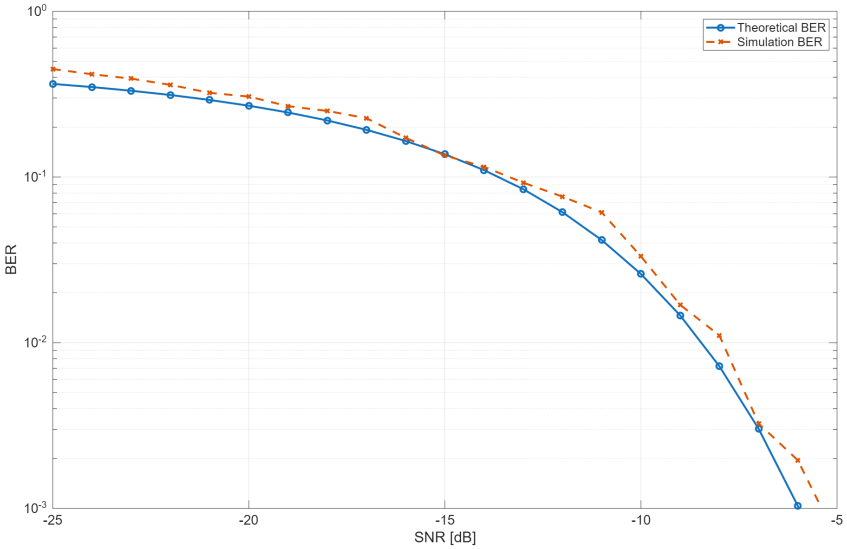


Figure 8. Comparison of simulated and theoretical communication BER results for $\varepsilon = 0.1$.

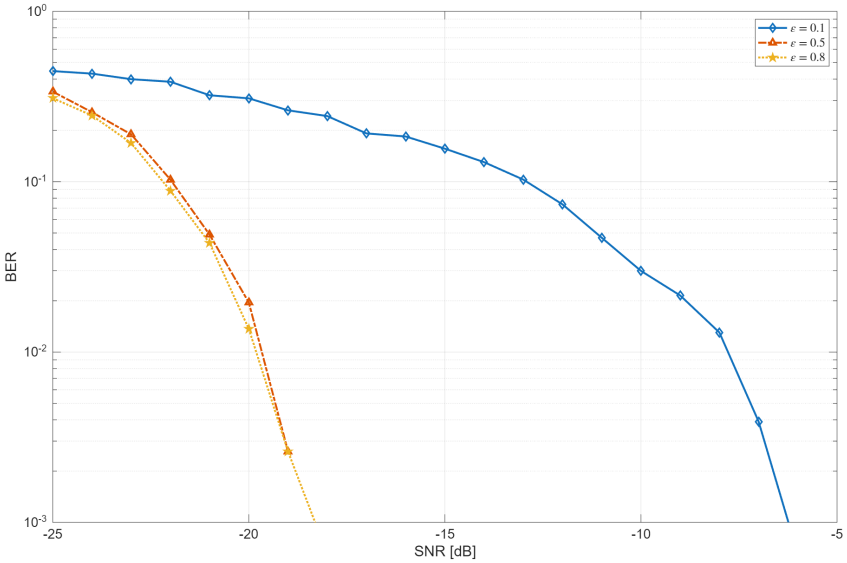


Figure 9. Communication BER results for $\varepsilon = 0.1$, $\varepsilon = 0.5$ and $\varepsilon = 0.8$.

Based on the imaging results in Section 7.2, the BER curve in Figure 9 shows the opposite effect of ε on these two abilities. For communication, increasing ε can improve BER performance. However, an increase in ε will generate stronger phase interference in the slow time dimension of the jamming signal, thereby reducing azimuth coherent focusing and deteriorating the sidelobe characteristics of false target image. This confirms

that ε is a key trade-off parameter for the proposed method. When jamming image quality is the main requirement, a smaller ε is preferred, while when communication reliability is more important and a certain degree of jamming image degradation can be accepted, a larger ε can be used.

To provide a reference comparison of the communication BER performance, the proposed method is compared with conventional OFDM and the methods reported in reference [32,35,36]. For the proposed method, we set $\varepsilon = 0.1$ and the SAR waveform parameters are kept the same as those listed in Table 1. The SNR range is set from -10 dB to 10 dB for simulation. For the reference methods, the main waveform and modulation parameters follow the settings in the corresponding references. Since these methods are based on different waveform structures and multiplexing mechanisms, their parameters cannot be made completely identical. Therefore, we aim to provide reference comparisons under representative parameter settings for each method, yielding the results shown in Figure 10. In the figure, the blue diamond line represents the result for conventional OFDM modulation, the red circle line represents the parameter modulation result proposed in reference [32], and the yellow pentagram and purple hexagon lines represent the results for FBMC-chirp and UFMC-chirp proposed in reference [35,36], respectively. The green cross line represents the result for the method proposed in this paper.

As shown in Figure 10, from the comparison, it can be seen that FBMC-chirp, UFMC-chirp, and conventional OFDM exhibit comparable performance. This is because these two methods share a similar basic principle with OFDM, allocating different subcarriers to accomplish jamming and communication tasks. In contrast, parameter modulation modulates communication information onto the time-domain and Doppler-domain parameters of the jamming signal to achieve information transmission, which also results in its BER performance being superior to that of FBMC-chirp and UFMC-chirp. Similarly, when using a matched filtering receiver, the method proposed in this paper achieved good BER performance. This is because the communication receiver can utilize jamming signals with known broadband LFM structures to obtain processing gain after matched filtering. It should be noted that the gain is related to the SAR waveform and receiver processing framework, not just the modulation format gain. And this also allows the BER to reach 10^{-3} even at a low SNR of -6 dB.

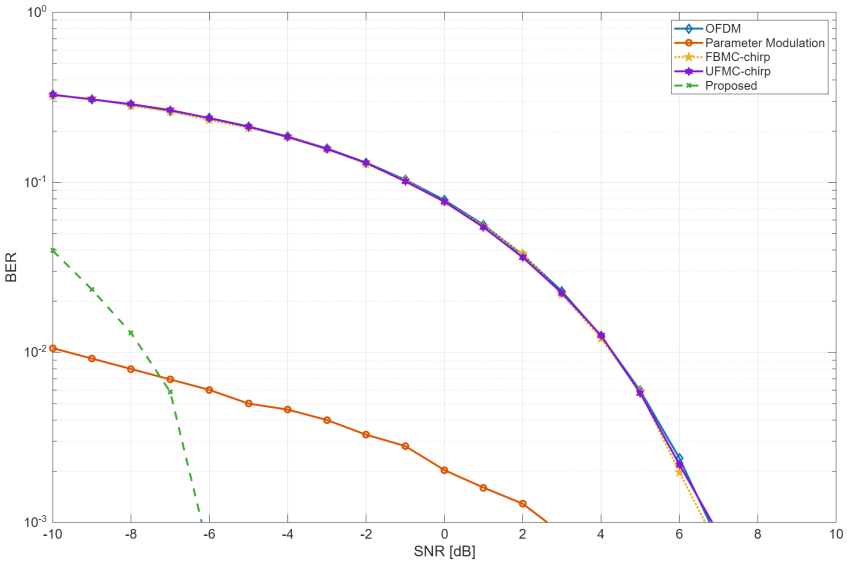


Figure 10. BER comparison results of OFDM, parameter modulation, FBMC-chirp, and UFMC-chirp methods.

8. Conclusions

This paper proposes a SAR SWJ multiplexing communication method based on small phase modulation. A detailed signal model is constructed around the proposed method and the communication modulation and demodulation algorithm flow is explained. The performance trade-off between jamming and communication is theoretically analyzed to ensure the feasibility of the method. Theoretical derivation and simulation experiments show that, in terms of jamming performance, compared with traditional SWJ, the proposed method does not significantly degrade its ability to construct false target jamming in SAR image, maintaining effective deception jamming. In terms of communication performance, communication receivers can utilize jamming signals with known broadband LFM structures to obtain processing gains after matched filtering. Enable it to exhibit excellent BER performance under lower SNR conditions.

It should be noted that this work is a preliminary exploration of SWJ multiplexing communication mechanism. Although the proposed method enables jamming signals to multiplex communication to a certain extent and achieves good BER performance, the slow time dimension of this information multiplexing means that the modulation of the information depends on the SAR radar parameters and imaging system of the UAV platform, which directly limits the achievable communication rate. Meanwhile, the channel model used in this paper is the AWGN model, in practical environments, although LOS occupies the main component; there may still be issues such as multipath reflection, which requires further discussion. Future work will focus on improving modulation methods and constructing multiple channel model analyses to further enhance overall performance and robustness in various scenarios.

Author Contributions: Conceptualization , B.Y., Q.Z., G.L. (Guidao Lin), Z.H. and G.L. (Gaogao Liu); Methodology, B.Y., Q.Z., J.C., G.L. (Gaogao Liu) and H.G.; Software, Q.Z., G.L. (Guidao Lin) and J.C.; Validation, B.Y., J.C. and Z.H.; Investigation, Q.Z.; Resources, G.L. (Guidao Lin); Writing—original draft, B.Y. and Q.Z.; Writing—review & editing, B.Y., Q.Z., G.L. (Guidao Lin), J.C., Z.H., G.L. (Gaogao Liu), H.G. and W.W.; Visualization, B.Y., Q.Z., G.L. (Guidao Lin), J.C. and Z.H.; Supervision, H.G. and W.W.; Project administration, B.Y., G.L. (Gaogao Liu) and H.G.; Funding acquisition, G.L. (Gaogao Liu). All authors have read and agreed to the published version of the manuscript.

Funding: This research received no external funding.

Data Availability Statement: The original contributions presented in this study are included in the article. Further inquiries can be directed to the corresponding author.

Conflicts of Interest: The authors declare no conflicts of interest.

References

1. Wang, W.-Q. MIMO SAR imaging: Potential and challenges. *IEEE Aerosp. Electron. Syst. Mag.* **2013**, *28*, 18–23. [CrossRef]
2. Krieger, G. MIMO-SAR: Opportunities and pitfalls. *IEEE Trans. Geosci. Remote Sens.* **2013**, *52*, 2628–2645. [CrossRef]
3. Zhang, Y.; Han, S.; Wei, T.; Wang, W.; Deng, Y.; Jin, G.; Zhang, Y.; Wang, R. First demonstration of echo separation for orthogonal waveform encoding MIMO-SAR based on airborne experiments. *IEEE Trans. Geosci. Remote Sens.* **2022**, *60*, 5225016. [CrossRef]
4. Wang, J.; Liang, X.-D.; Chen, L.-Y.; Li, Y.-L. First demonstration of airborne MIMO SAR system for multimodal operation. *IEEE Trans. Geosci. Remote Sens.* **2021**, *60*, 5204113. [CrossRef]
5. Wei, Y.; Zhang, Y.; Liu, Y.; Wang, W.; Wang, P.; Deng, Y.; Peng, W.; Zhang, Z.; Wang, Z.; Liu, R. Elevation-Interpulse Phase Coded Waveform: A Novel Radar Waveform for Spaceborne MIMO-SAR. *IEEE Trans. Geosci. Remote. Sens.* **2025**, *63*, 5213818 . [CrossRef]
6. Liu, B.; He, Y.; Li, X. A new concept of full ocean current vector retrieval with spaceborne SAR based on intrapulse beam-switching technique. *IEEE Trans. Geosci. Remote Sens.* **2020**, *58*, 7682–7704. [CrossRef]
7. Wang, Y.; Jin, G.; Song, C.; Lu, P.; Han, S.; Lv, J.; Zhang, Y.; Wu, D.; Zhu, D. Parameterized and large-dynamic-range 2-D precise controllable SAR jamming: Characterization, modeling, and analysis. *IEEE Trans. Geosci. Remote Sens.* **2023**, *61*, 5209416.

8. Zhou, F.; Zhao, B.; Tao, M.; Bai, X.; Chen, B.; Sun, G. A large scene deceptive jamming method for space-borne SAR. *IEEE Trans. Geosci. Remote Sens.* **2013**, *51*, 4486–4495. [CrossRef]
9. Ji, P.; Xing, S.; Dai, D.; Pang, B.; Feng, D. A template-modulation jamming against SAR based on frequency-diverse array. *IEEE Geosci. Remote Sens. Lett.* **2023**, *20*, 4014405.
10. Li, N.-J.; Zhang, Y.-T. A survey of radar ECM and ECCM. *IEEE Trans. Aerosp. Electron. Syst.* **1995**, *31*, 1110–1120. [CrossRef]
11. Xu, H.; Quan, Y.; Zhou, X.; Chen, H.; Cui, T.J. A novel approach for radar passive jamming based on multiphase coding rapid modulation. *IEEE Trans. Geosci. Remote Sens.* **2023**, *61*, 5101614. [CrossRef]
12. Gibert, F.; Gómez-Olivé, A.; Garcia-Mondéjar, A.; Francis, R.; Hernández, S.; De La Cruz, A.F.; Vendrell, E.; i Aparici, M.R. A trihedral corner reflector for radar altimeter calibration. *IEEE Trans. Geosci. Remote Sens.* **2023**, *61*, 5101408. [CrossRef]
13. Gan, L.; Wu, Z.; Li, J. A Passive ISAR Jamming Method Based on Time-Modulated Corner Reflectors Under Asynchronous Control. *IEEE Trans. Aerosp. Electron. Syst.* **2025**, *61*, 11103–11115. [CrossRef]
14. Shi, Q.; Huang, J.; Xie, T.; Wang, C.; Yuan, N. An active jamming method against ISAR based on periodic binary phase modulation. *IEEE Sens. J.* **2019**, *19*, 7950–7960. [CrossRef]
15. Wang, Y.; Jin, G.; Shi, T.; Ma, R.; Zhang, Y.; Wu, D.; Zhu, D. Knowledge-aided precise jamming technique against spaceborne SAR system. *IEEE Trans. Aerosp. Electron. Syst.* **2024**, *60*, 2791–2806. [CrossRef]
16. Zhang, Z.; Li, X.; Li, Y.; Zhang, T.; Xia, X. Joint Optimization of Node Positions and Transmit States for Distributed MIMO Surveillance in Electronic Countermeasure Environments. *IEEE Trans. Aerosp. Electron. Syst.* **2026**, *62*, 4663–4677. [CrossRef]
17. Zhou, F.; Sun, G.; Bai, X.; Bao, Z. A novel method for adaptive SAR barrage jamming suppression. *IEEE Geosci. Remote Sens. Lett.* **2011**, *9*, 292–296. [CrossRef]
18. Cheng, S.; Zheng, H.; Yu, W.; Lv, Z.; Chen, Z.; Qiu, T. A barrage jamming suppression scheme for DBF-SAR system based on elevation multichannel cancellation. *IEEE Geosci. Remote Sens. Lett.* **2023**, *20*, 4008305. [CrossRef]
19. Li, N.; Cheng, D.; Lu, P.; Shu, G.; Guo, Z. Smart jamming against SAR based on nonlinear frequency-modulated signal. *IEEE Trans. Aerosp. Electron. Syst.* **2022**, *59*, 3588–3605. [CrossRef]
20. Liu, Z.; Cheng, D.; Li, N.; Min, L.; Guo, Z. Two-dimensional precise controllable smart jamming against SAR via phase errors modulation of transmitted signal. *IEEE Geosci. Remote Sens. Lett.* **2023**, *21*, 4000705. [CrossRef]
21. Feng, D.; Xu, L.; Pan, X.; Wang, X. Jamming wideband radar using interrupted-sampling repeater. *IEEE Trans. Aerosp. Electron. Syst.* **2017**, *53*, 1341–1354. [CrossRef]
22. Wu, W.; Zou, J.; Chen, J.; Xu, S.; Chen, Z. False-target recognition against interrupted-sampling repeater jamming based on integration decomposition. *IEEE Trans. Aerosp. Electron. Syst.* **2021**, *57*, 2979–2991.
23. Zhou, K.; Su, Y.; Wang, D.; Ma, H.; Liu, L.; Li, C. Improved SAR interrupted-sampling repeater jamming countermeasure based on waveform agility and mismatched filter design. *IEEE Trans. Geosci. Remote Sens.* **2023**, *61*, 5206916. [CrossRef]
24. Liu, Y.-X.; Zhang, Q.; Xiong, S.-C.; Wang, H.-B.; Yuan, H.; Luo, Y. A Multiple-False-Target ISAR Shape Deception Jamming Method Based on Improved Template Multiplication Modulated Time-Delay Algorithm and Sub-Nyquist Sampling. *Remote Sens.* **2023**, *15*, 5015.
25. Gao, X.-P.; Lei, W.-H. Method of implementing scatter-wave jamming signal to SAR. *Mod. Radar* **2006**, *8* , 22–24.
26. Li, T.; Chen, W.; Lu, G.; Wang, D. A study on scatter-wave jamming for countering SAR. In *Proceedings of the 2007 International Conference on Microwave and Millimeter Wave Technology*; IEEE: New York, NY, USA, 2007; pp. 1–4.
27. Jia, M.; Sun, Y.; Wang, W.-Q. FDA-MIMO radar parameter designing against range-ambiguous clutter and scatter-wave jamming. *Signal Process.* **2025**, *240* , 110361.
28. Zhao, B.; Zhou, F.; Tao, M.; Zhang, Z.; Bao, Z. Improved method for synthetic aperture radar scattered wave deception jamming. *IET Radar Sonar Navig.* **2014**, *8*, 971–976. [CrossRef]
29. Dong, C.; Chang, X. A novel scattered wave deception jamming against three channel SAR GMTI. *IEEE Access* **2018**, *6*, 53882–53889. [CrossRef]
30. Huang, B.; Wang, W.-Q.; Zhang, S.; Wang, H.; Gui, R.; Lu, Z. A novel approach for spaceborne SAR scattered-wave deception jamming using frequency diverse array. *IEEE Geosci. Remote Sens. Lett.* **2019**, *17*, 1568–1572. [CrossRef]
31. Guo, J.; Wang, Y. SAR scatter-wave jamming based on LFMCW product modulation. *IEEE Geosci. Remote Sens. Lett.* **2023**, *20*, 4007605. [CrossRef]
32. Liu, G.; Yang, W.; Wang, Y.; Wang, Z.; Huang, D.; Li, P.; Bao, D.; Man, X.; Wu, B. Joint communication interference system design based on parameter modulation. *Appl. Opt.* **2022**, *61*, 1057–1067. [CrossRef] [PubMed]
33. Lotfi, I.; Du, H.; Niyato, D.; Sun, S.; Kim, D.I. On the robustness of channel allocation in joint radar and communication systems: An auction approach. *IEEE Trans. Mob. Comput.* **2023**, *23*, 3466–3483. [CrossRef]
34. Bekar, M.; Baker, C.J.; Hoare, E.G.; Gashinova, M. Joint MIMO radar and communication system using a PSK-LFM waveform with TDM and CDM approaches. *IEEE Sens. J.* **2020**, *21*, 6115–6124. [CrossRef]

35. Liu, G.; Yang, W.; Bao, Y.; Wang, Y.; Li, P. Joint communication and jamming system design based on filter bank multicarrier chirp waveform: Using for curvilinear flight scenario. *Remote Sens.* **2023**, *15*, 1239. [CrossRef]
36. Liu, G.; Huang, Z.; Zhang, Q.; Mu, B.; Guo, H. Joint radar jamming and communication system design based on universal filtered multicarrier chirp waveform. *Remote Sens.* **2024**, *16*, 1383. [CrossRef]

Disclaimer/Publisher's Note: The statements, opinions and data contained in all publications are solely those of the individual author(s) and contributor(s) and not of MDPI and/or the editor(s). MDPI and/or the editor(s) disclaim responsibility for any injury to people or property resulting from any ideas, methods, instructions or products referred to in the content.